Schweizerischer Erdbebendienst
Service Sismologique Suisse
Servizio Sismico Svizzero
Servizi da Terratrembels Svizzer

ETH
Eidgenössische Technische Hochschule Zürich
Swiss Federal Institute of Technology Zurich

Brig - Spital (SBRS)

SITE CHARACTERIZATION REPORT

Clotaire MICHEL, Jan BURJANEK, Daniel ROTEN

Valerio POGGI, Carlo CAUZZI, Donat FÄH

Sonneggstrasse 5 CH-8092 Zürich Switzerland; E-mail: clotaire.michel@sed.ethz.ch

Last modified : November 5, 2013

Abstract

Ambient vibration array measurements were performed to characterize the sedimentary deposits at site Brig Spital. The site, where the new station SBRS of the Swiss Strong Motion Network was installed, is located in the Rhone valley. SBRS replaces the dial-up station SBRG. In order to characterize the velocity profile under the station, array measurements with a $200\,\mathrm{m}$ aperture were performed. The measurements were successful and allowed deriving a velocity model for this site. The soil column underlying station SBRS is made of 1 to $3\,\mathrm{m}$ with a larger velocity than the lower layers. The velocity remains low until $5\,\mathrm{m}$ depth (badly constrained) and then increases from 300 to $850\,\mathrm{m/s}$ at $20\,\mathrm{m}$ depth. In the lower layers, only a slight increase up to $1000\,\mathrm{m/s}$ is found until the bedrock between around $200\,\mathrm{m}$ with the imposed velocity of $2600\,\mathrm{m/s}$. $V_{s,30}$ is $386\,\mathrm{m/s}$. The ground type is C for EC8 [CEN, 2004], and E for SIA261 [SIA, 2003]. The theoretical SH transfer function and impedance contrast of the quarter-wavelength velocity computed from the inverted profiles show a large amplification especially at the resonance frequencies 3 and $4.5\,\mathrm{Hz}$. Recordings on the new station will allow to validate these simple models and recognize if 2D resonance occurs or not.

Contents

1 Introduction

The station SBRS (Brig - Spital) is part of the Swiss Strong Motion Network (SSMNet) in the Rhone valley. SBRS has been installed in the framework of the SSMNet Renewal project in 2012 as a replacement for dial-up station SBRG. This project includes also the site characterization. Passive array measurements have been selected as a standard tool to investigate these sites. An array measurement campaign was carried out on 24th October 2012 in a field behind the hospital of Brig (Fig. 1), with a centre close to station SBRS, in order to characterize the sediments under this station. The city of Brig suffered heavy damage during several historical earthquakes, especially the M 6 earthquake in 1755. According to the geological map, this station is located on the alluvial fan of the Saltina river and the deep alluvia of the Rhone river. Boreholes in the surroundings (valley roads) show a majority of gravels in the first $30\,\mathrm{m}$. This report presents the measurement setup, the results of the H/V analysis and of the array processing of the surface waves (dispersion curves). Then, an inversion of these results into velocity profiles is performed. Standard parameters are derived to evaluate the amplification at this site.

Canton	City	Location	Station code	Site type	Slope
Valais	Brig	Spital	SBRS	Deep valley	Flat

Table 1: Main characteristics of the study-site.

Figure 1: Picture of the site.

2 Experiment description

2.1 Ambient Vibrations

The ground surface is permanently subjected to ambient vibrations due to:

- natural sources (ocean and large-scale atmospheric phenomena) below $1\,\mathrm{Hz}$,
- local meteorological conditions (wind and rain) at frequencies around $1\,\mathrm{Hz}$,
- human activities (industrial machines, traffic…) at frequencies above $1\,\mathrm{Hz}$ [Bonnefoy-Claudet et al., 2006].

The objective of the measurements is to record these ambient vibrations and to use their propagation properties to infer the underground structure. First, the polarization of the recorded waves (H/V ratio) is used to derive the resonance frequencies of the soil column. Second, the phase delays at many different stations are used to derive the velocity of surface waves at different frequencies (dispersion). The information (H/V, dispersion curves) is then used to derive the properties of the soil column using an inversion process.

2.2 Equipment

For these measurements 12 Quanterra Q330 dataloggers named NR01 to NR12 and 14 Lennartz 3C 5 s seismometers were available (see Tab. 2). Each datalogger can record on 2 ports A (channels EH1, EH2, EH3 for Z, N, E directions) and B (channels EH4, EH5, EH6 for Z, N, E directions). Time synchronization was ensured by GPS. The sensors were placed on a metal tripod in a $20\,\mathrm{cm}$ deep hole, when possible, for better coupling with the ground.

Digitizer	**Model**	**Number**	**Resolution**
	Quanterra Q330	12	$24\,\mathrm{bits}$
Sensor type	**Model**	**Number**	**Cut-off frequency**
Velocimeter	Lennartz 3C	14	$0.2\,\mathrm{Hz}$

Table 2: Equipment used.

2.3 Geometry of the arrays

Two array configurations were used, for a total of 4 rings of 10, 25, 50 and $100\,\mathrm{m}$ radius around a central station. The first configuration includes the 3 inner rings with 14 sensors; the second configuration includes the 2 outer rings (plus the first ring) with 14 sensors. The minimum inter-station distance and the aperture are therefore 10 and $100\,\mathrm{m}$ and 10 and $200\,\mathrm{m}$, respectively. The experimental setup is displayed in Fig. 2. The final usable datasets are detailed in section 3.2.

Figure 2: Geometry of the arrays.

2.4 Positioning of the stations

The sensor coordinates were measured using a differential GPS device (Leica Viva GS10), including only a rover station and using the Real Time Kinematic technique provided by Swisstopo. It allowed an absolute positioning with an accuracy better than $5\,\mathrm{cm}$ on the Swissgrid.

3 Data quality

3.1 Usable data

The largest time windows were extracted, for which all the sensors of the array were correctly placed and the GPS synchronization was ensured. The array was limited in size by a main road and the highway, parallel to the train line.

Points BRS402 and especially BRS405, located along these main roads show therefore much higher noise levels at low frequencies due to the air flow on the sensor. At higher frequencies, the effect of the road proximity can only be seen on station BRS405, located really close to a road where cars are driving fast ($\approx 70\,\mathrm{km/h}$). The vertical spectrum at this station shows a relatively narrow peak, centered around $16\,\mathrm{Hz}$ (higher frequencies compared to the others where the peak of the anthropogenic ambient noise is around $10\,\mathrm{Hz}$) and is most probably caused by the traffic. For the other stations, even along roads, this part of the spectra is comparable indicating that many sources contribute to ambient vibrations at these frequencies.
Moreover, a small road was crossing the array with numerous cars, tractors and panzers passing by. Points BRS205, BRS301, BRS305 and BRS401, located along this road, show a slightly higher noise level at low frequencies, maybe due to the air flow. Again, this disturbance cannot be seen at higher frequencies. GPS measurement were not performed during the recordings to avoid additional disturbances.

Moreover, spurious frequency peaks are detected at various frequencies (1.08, 2.48, 3.6, $3.7\,\mathrm{Hz}$) on all recordings, as well as at 4.3, 16.1 and $17.3\,\mathrm{Hz}$ on some recordings.

Orientations of the sensors were checked by maximizing the correlation with the central station at low frequencies [Poggi et al., 2012b]. Deviations lower than $8\,^\circ$ were found for all points. Original and rotated datasets are available for the 3C array analysis.

The characteristics of the datasets are detailed in Tab. 3.

3.2 Data processing

The data were first converted to SAC format including in the header the coordinates of the point (CH1903 system), the recording component and a name related to the position. The name is made of 3 letters characterizing the location (BRS here), 1 digit for the ring and 2 more digits for the number in the ring. Recordings were not corrected for instrumental response.

Dataset	Starting Date	Time	Length	F_s	Min. inter-distance	Aperture	# of points
1	2012/10/24	10:35	118 min	200 Hz	10 m	100 m	14
2	2012/10/24	12:58	141 min	200 Hz	10 m	200 m	14

Table 3: Usable datasets.

4 H/V processing

4.1 Processing method and parameters

In order to process the H/V spectral ratios, several codes and methods were used. The classical H/V method was applied using the Geopsy `http://www.geopsy.org` software. In this method, the ratio of the smoothed Fourier Transform of selected time windows are averaged. Tukey windows (cosine taper of 5% width) of $50\,\mathrm{s}$ long overlapping by 50% were selected. Konno and Ohmachi [1998] smoothing procedure was used with a b value of 60. The classical method computed using the method of Fäh et al. [2001] was also performed.

Moreover, the time-frequency analysis method [Fäh et al., 2009] was used to estimate the ellipticity function more accurately using the Matlab code of V. Poggi. In this method, the time-frequency analysis using the Wavelet transform is computed for each component. For each frequency, the maxima over time (10 per minute with at least $0.1\,\mathrm{s}$ between each) in the TFA are determined. The Horizontal to Vertical ratio of amplitudes for each maximum is then computed and statistical properties for each frequency are derived. A Cosine wavelet with parameter 9 is used [Poggi et al., 2012b]. The mean of the distribution for each frequency is stored. For the sake of comparison, the time-frequency analysis of Fäh et al. [2001], based on the spectrogram, was also used, as well as the wavelet-based TFA coded in Geopsy.

The ellipticity extraction using the Capon analysis [Poggi and Fäh, 2010] (see section on array analysis) was also performed.

Method	Freq. band	Win. length	Anti-trig.	Overlap	Smoothing
Standard H/V Geopsy	$0.2-20\,\mathrm{Hz}$	$50\,\mathrm{s}$	No	50%	K&O 60
Standard H/V D. Fäh	$0.2-20\,\mathrm{Hz}$	$30\,\mathrm{s}$	No	75%	-
H/V TFA Geopsy	$0.2-20\,\mathrm{Hz}$	Morlet m=8 fi=1	No	-	-
H/V TFA D. Fäh	$0.2-20\,\mathrm{Hz}$	Specgram	No	-	-
H/V TFA V. Poggi	$0.2-20\,\mathrm{Hz}$	Cosine wpar=9	No	-	No

Table 4: Methods and parameters used for the H/V processing.

4.2 Results

Most of the points show a similar shape in their H/V with a fundamental peak around $1.3-1.4\,\mathrm{Hz}$ and a second double bump around $4\,\mathrm{Hz}$. Only point BRS402 differs largely from this shape. Point BRS405 and BRS404 also show a peak with lower amplitude.

Moreover, all the methods to compute H/V ratios are compared at the array centre on Fig. 4, in which the classical methods were divided by $\sqrt{2}$ to correct from the Love wave contribution [Fäh et al., 2001]. The classical and TFA methods match well at high frequencies but the fundamental peak value and amplitude vary for each method. The 3C FK analysis (Capon method) does not have resolution down to the peak and matches roughly, maybe due to lateral variability.

Looking at the H/V fundamental frequency map of the array (Fig. 5), it seems that the array is located on a homogeneous zone with a fundamental frequency of $1.35\,\mathrm{Hz}$ but the extent of this zone is rather limited. In the North, the fundamental frequency increases rapidly in the basin edge (BRS402), in the South, the frequency starts to decrease at the edge of the array (BRS405). Station SBRS and the hospital site is therefore well characterized by the array, but the site conditions may be rather different in other parts of the city. On the contrary to the cities downstream, this part of the Rhone valley is not covered by measurements.

On Fig. 6, these results are compared to the H/V computed on long term recordings at new station SBRS and test station XBRG1. It should be noticed that H/V at SBRS is not reliable below $2\,\mathrm{Hz}$ due to the noise of the acquisition chain (strong-motion instrument). XBRG1 was installed inside the hospital building whereas SBRS is located outside in a concrete pot. The H/V curve is comparable to the array results except for a double peak at 2.61 and $2.91\,\mathrm{Hz}$ that appears especially on XBRG1 and that is related to the building resonance. It can be noticed that the pot installation reduced the effect of the building on the recorded motion but does not annihilate it.

The peak at the SBRS station is therefore at $1.4\,\mathrm{Hz}$, with a peak amplitude around 4 for the TFA methods.

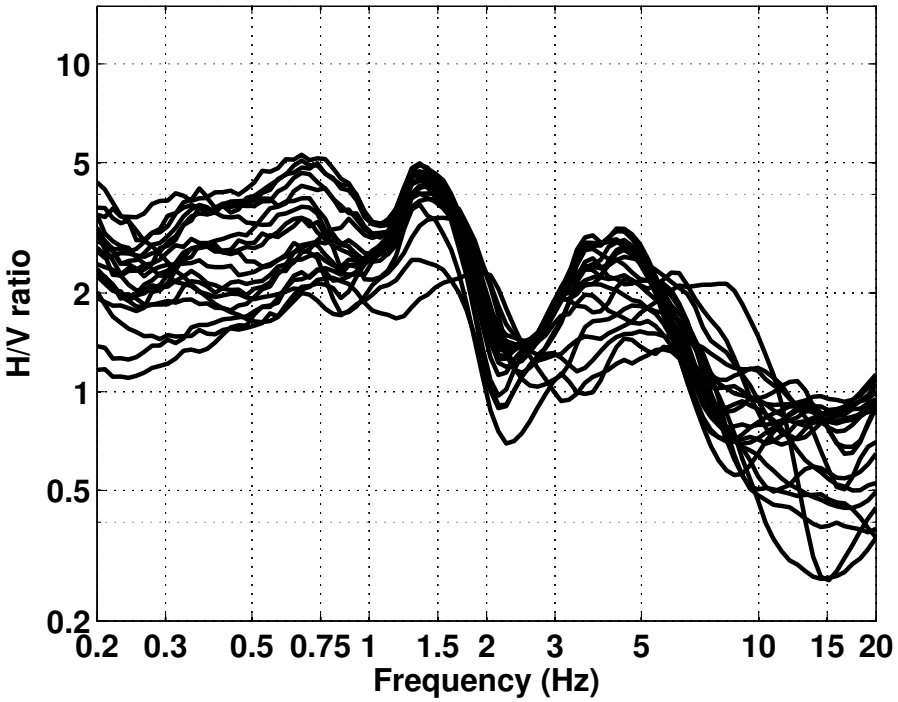

Figure 3: H/V spectral ratios (time-frequency analysis code V. Poggi).

4.3 Polarization analysis

Considering the shape of the Rhone basin, a 2D resonance could occur. Therefore, polarization analysis on the array data was performed using the method of Burjánek et al. [2010]. All points

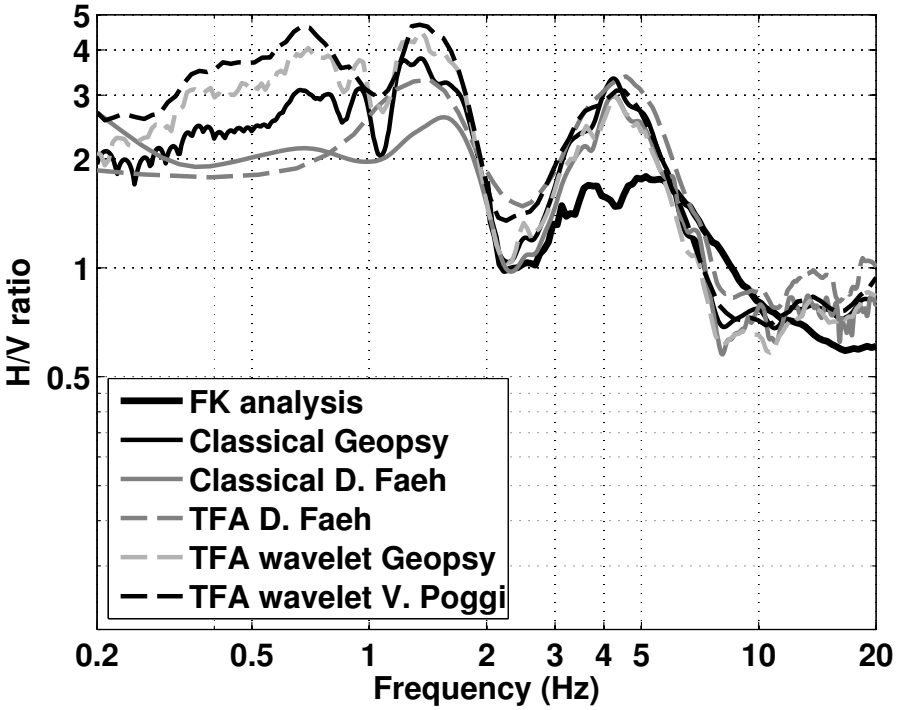

Figure 4: H/V spectral ratios for point BRS000 using the different codes. Classical methods were divided by $\sqrt{2}$.

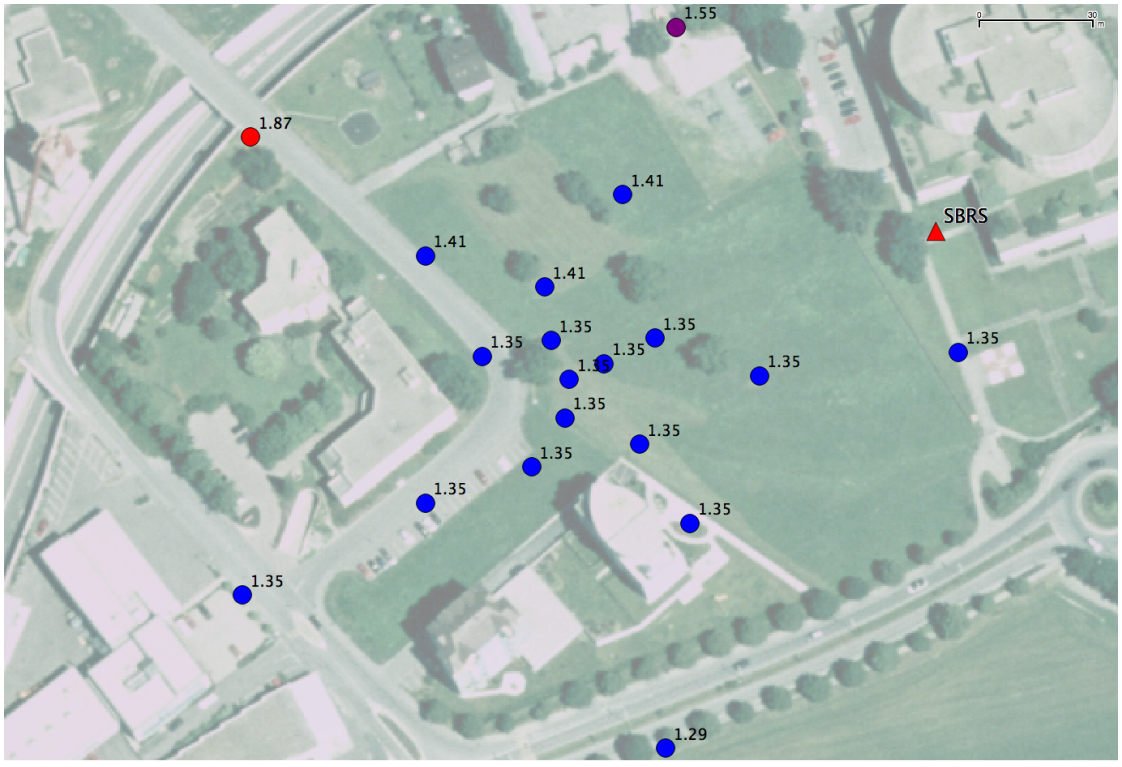

Figure 5: Map of the H/V resonance frequency in the array.

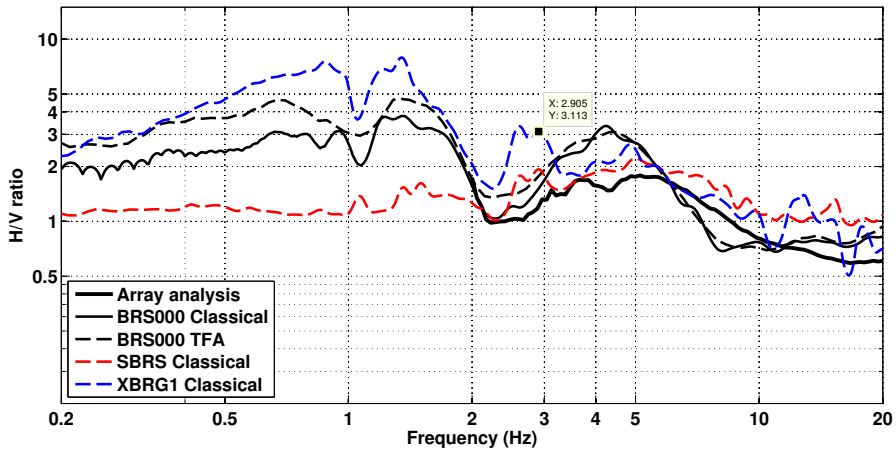

Figure 6: H/V spectral ratios at point BRS000, for the whole array (FK method), at SBRS station (not reliable below 2 Hz) and at XBRG1 test station.

(Fig. 7) show a polarization at 1.3 Hz in a direction close to the valley axis (37 °N, see maps on Fig. 8). It is different from the main valley axis but parallel to the bedrock slope close to the array. It is therefore not excluded that this resonance frequency is related to 2D behaviour of the valley.

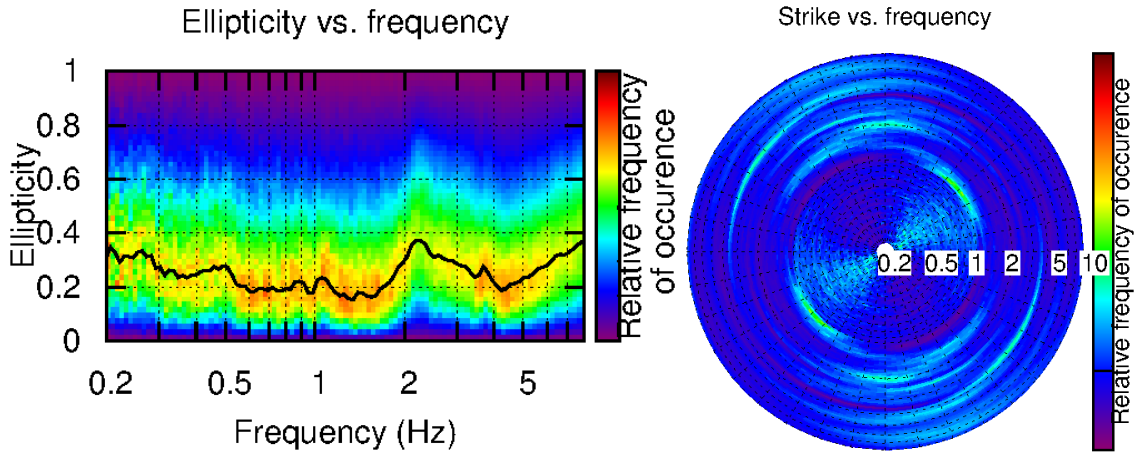

Figure 7: Polarization analysis at point BRS000. Left: Ellipticity (A trough in the ellipticity corresponds to polarized motion). Right: Strike of the polarization.

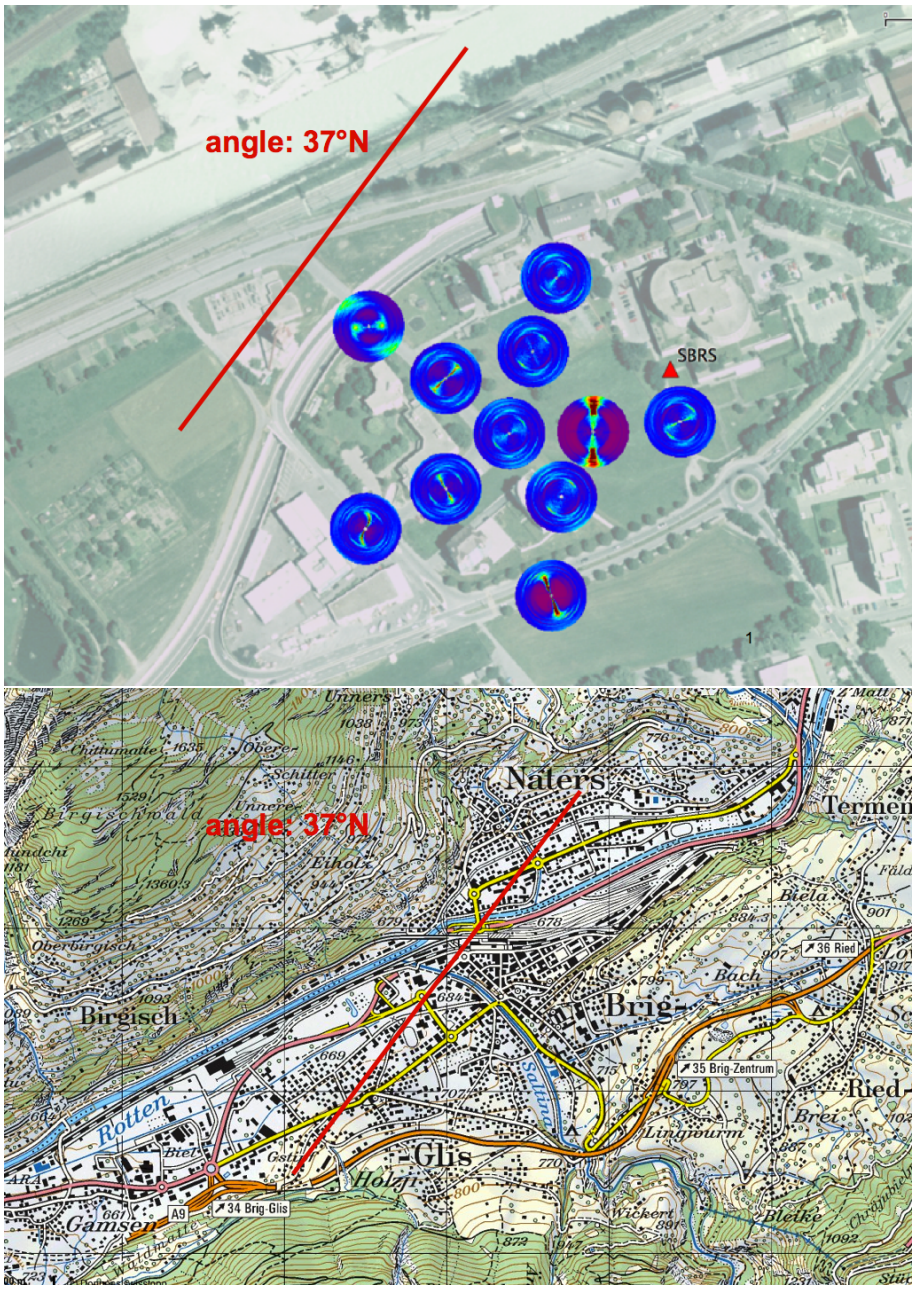

Figure 8: Map of the strike of the polarization (top) and overview map of the Rhone valley at Brig site (bottom).

5 Array processing

5.1 Processing methods and parameters

The vertical components of the arrays were processed using the FK and the High-resolution FK analysis [Capon, 1969] using the Geopsy `http://www.geopsy.org` software. Better results were obtained using large time windows (300T). The results of computations of both datasets were merged to estimate the dispersion curves.

Moreover, a 3C array analysis [Fäh et al., 2008] was also performed using the array_tool_3C software [Poggi and Fäh, 2010]. It allows to derive Rayleigh and Love modes including the Rayleigh ellipticity. The results of computations of both datasets were merged to estimate the dispersion curves.

Method	Set	Freq. band	Win. length	Anti-trig.	Overlap	Grid step	Grid size	# max.
HRFK 1C	1	$1-20\,\mathrm{Hz}$	$300T$	No	50%	0.001	0.6	5
HRFK 1C	2	$1-20\,\mathrm{Hz}$	$300T$	No	50%	0.001	0.6	5
HRFK 3C	1	$1.5-20\,\mathrm{Hz}$	Wav. 10 Tap. 0.2	No	50%	150 m/s	2000 m/s	5
HRFK 3C	2	$1.5-20\,\mathrm{Hz}$	Wav. 10 Tap. 0.2	No	50%	150 m/s	2000 m/s	5

Table 5: Methods and parameters used for the array processing.

5.2 Obtained dispersion curves

The first Rayleigh mode in the 1C FK analysis could be picked between 2 and $10.5\,\mathrm{Hz}$ (Fig. 9) including its standard deviation and further to $16.5\,\mathrm{Hz}$ without standard deviation. The velocities are ranging from $1500\,\mathrm{m/s}$ at $2\,\mathrm{Hz}$ down to $190\,\mathrm{m/s}$ at $16.5\,\mathrm{Hz}$.

Using the 3C analysis, both fundamental Rayleigh and Love modes can be picked (Fig. 9). Love fundamental mode is picked from 2.4 to $20\,\mathrm{Hz}$ (Fig. 10). The first higher Love mode is also picked from the transverse component. Moreover, the radial component provides the Rayleigh first higher mode. The fundamental Rayleigh mode shows no difference with the 1C analysis (Fig. 10). However, looking at the radial component, the picking of the fundamental Rayleigh mode is debatable and may be influenced by the first higher mode.

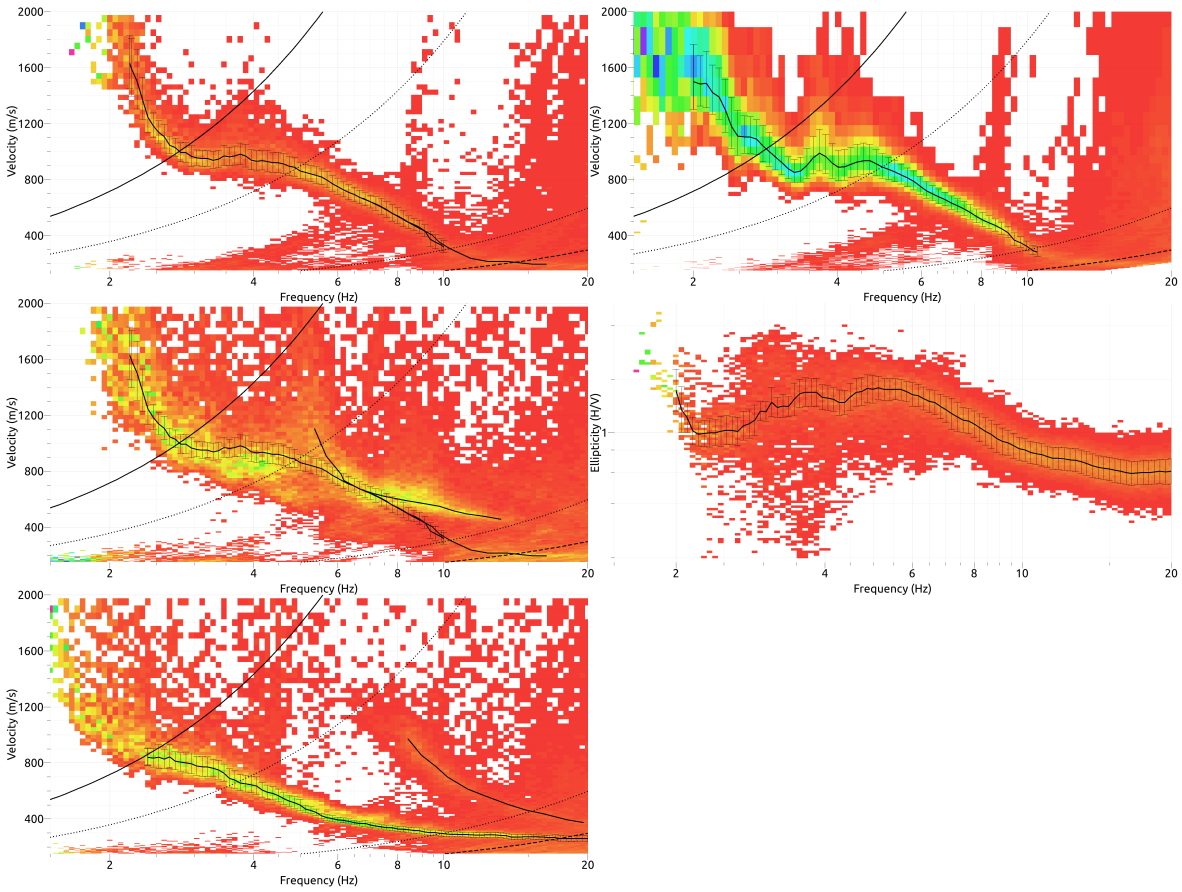

Figure 9: Dispersion curves obtained from the 3C (left) and 1C (top right) array analysis (top: vertical; centre: radial; bottom: transverse components) and ellipticity from 3C analysis (centre right).

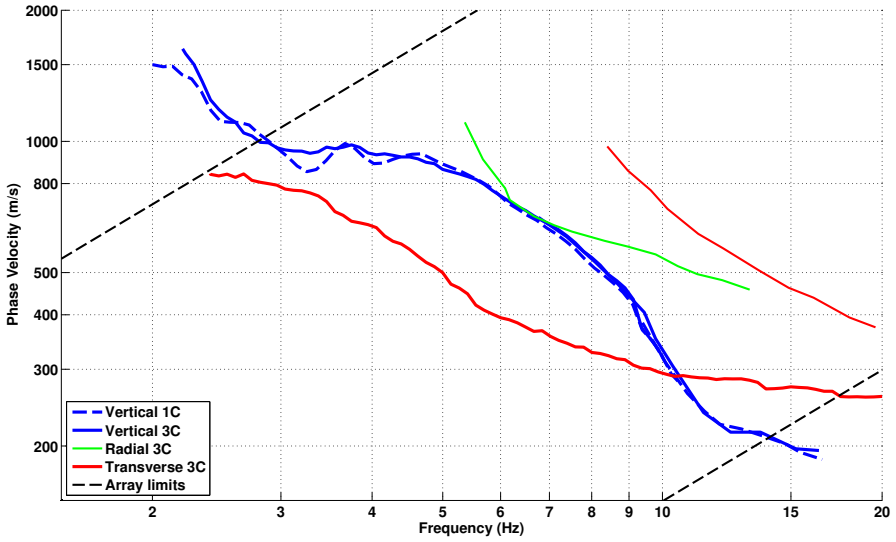

Figure 10: Picked dispersion curves from 1C and 3C FK methods.

6 Inversion and interpretation

6.1 Inversion

For the inversion, Rayleigh and Love fundamental and their first higher modes dispersion curves without standard deviation to avoid different weighting and the fundamental peak at $1.4\,\mathrm{Hz}$ were used as simultaneous targets. All curves were resampled using 50 points between 1 and $20\,\mathrm{Hz}$ in log scale. The right flank of the ellipticity of the Rayleigh waves is displayed in the results but was not used in the inversion. The fundamental and first higher Rayleigh modes were not used in the frequency bands $3 - 7.5\,\mathrm{Hz}$ and $5.9 - 9\,\mathrm{Hz}$, respectively, because the picked curves are affected by a mix of these modes.

The inversion was performed using the Improved Neighborhood Algorithm (NA) Wathelet [2008] implemented in the Dinver software. In this algorithm, the tuning parameters are the following: Ns_0 is the number of starting models, randomly distributed in the parameter space, Nr is the the number of best cells considered around these Ns_0 models, Ns is the number of new cells generated in the neighborhood of the Nr cells (Ns/Nr per cell) and It_{max} is the number of iteration of this process. The process ends with $Ns_0 + Nr * \frac{Ns}{Nr} * It_{max}$ models. The used parameters are detailed in Tab. 6.

It_{max}	Ns_0	Ns	Nr
500	10000	100	100

Table 6: Tuning parameters of Neighborhood Algorithm.

During the inversion process, low velocity zones were not allowed except for the first interface that allows a better fit at high frequencies. The bedrock velocity is set at $2600\,\mathrm{m/s}$, which turns out to be a good compromise between data fit and observation of amplification at the strong motion station. The bedrock depth had also to be set in a narrow range ($190 - 210\,\mathrm{m}$ depth for the free layer depth parameterizations) for the same reasons. It should be noticed that this inversion is very sensitive to the targets used that is why so many assumptions had to be made to avoid unrealistic results. The Poisson ratio was inverted in each layer in the range 0.2-0.4, up to 0.47 just below the expected water table. The density was supposed equal to $2000\,\mathrm{kg/m^3}$ except for the deepest layer ($2500\,\mathrm{kg/m^3}$). Inversions with free layer depths as well as fixed layer depths were performed. 4 layers are enough to explain most of the targets (dispersion and ellipticity), but more layers are used to smooth the obtained results and better explore the parameter space. 5 independent runs of 5 different parametrization schemes (5 and 6 layers over a half space and 11, 13 and 15 layers with fixed depth) were performed. For further elaborations, the best models of these 25 runs were selected (Fig. 14).

The first 1 to $3\,\mathrm{m}$ show a larger velocity than the lower layers around $400\,\mathrm{m/s}$ (Fig. 11 and Fig. 14). Below the velocity remains extremely low until $5\,\mathrm{m}$ depth (badly constrained) and then increases from 300 to $850\,\mathrm{m/s}$ at $20\,\mathrm{m}$ depth. It then increases slightly to $1000\,\mathrm{m/s}$ until the bedrock between 160 and $210\,\mathrm{m}$ with the imposed velocity of $2600\,\mathrm{m/s}$.

When comparing to the target curves (Fig. 12 and Fig. 13), all curves are well represented.

These results are compatible with the 3D model of Visp, downstream, proposed by Fäh et al.

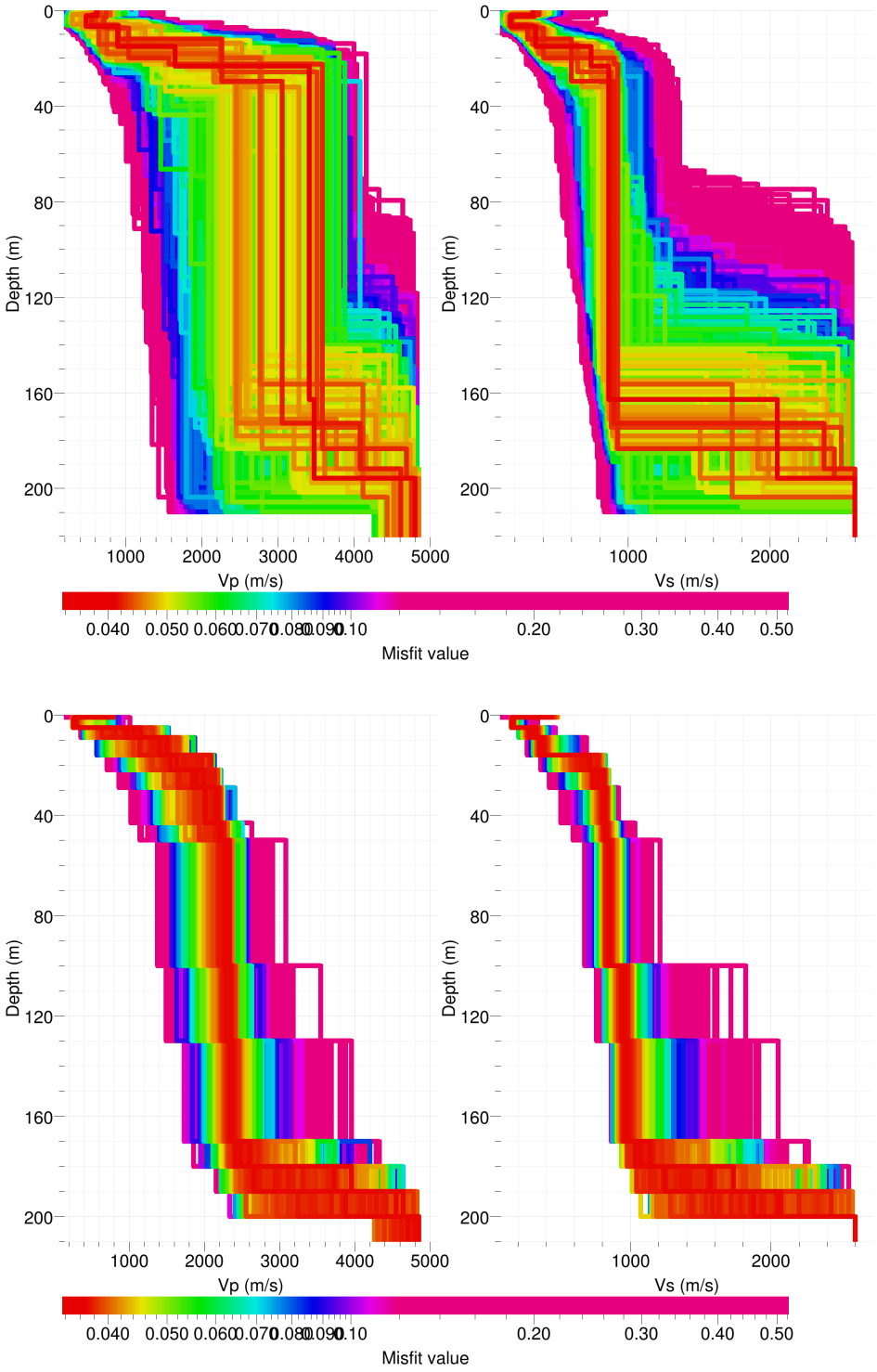

Figure 11: Inverted ground profiles in terms of V_p and V_s; top: free layer depth strategy; bottom: fixed layer depth strategy.

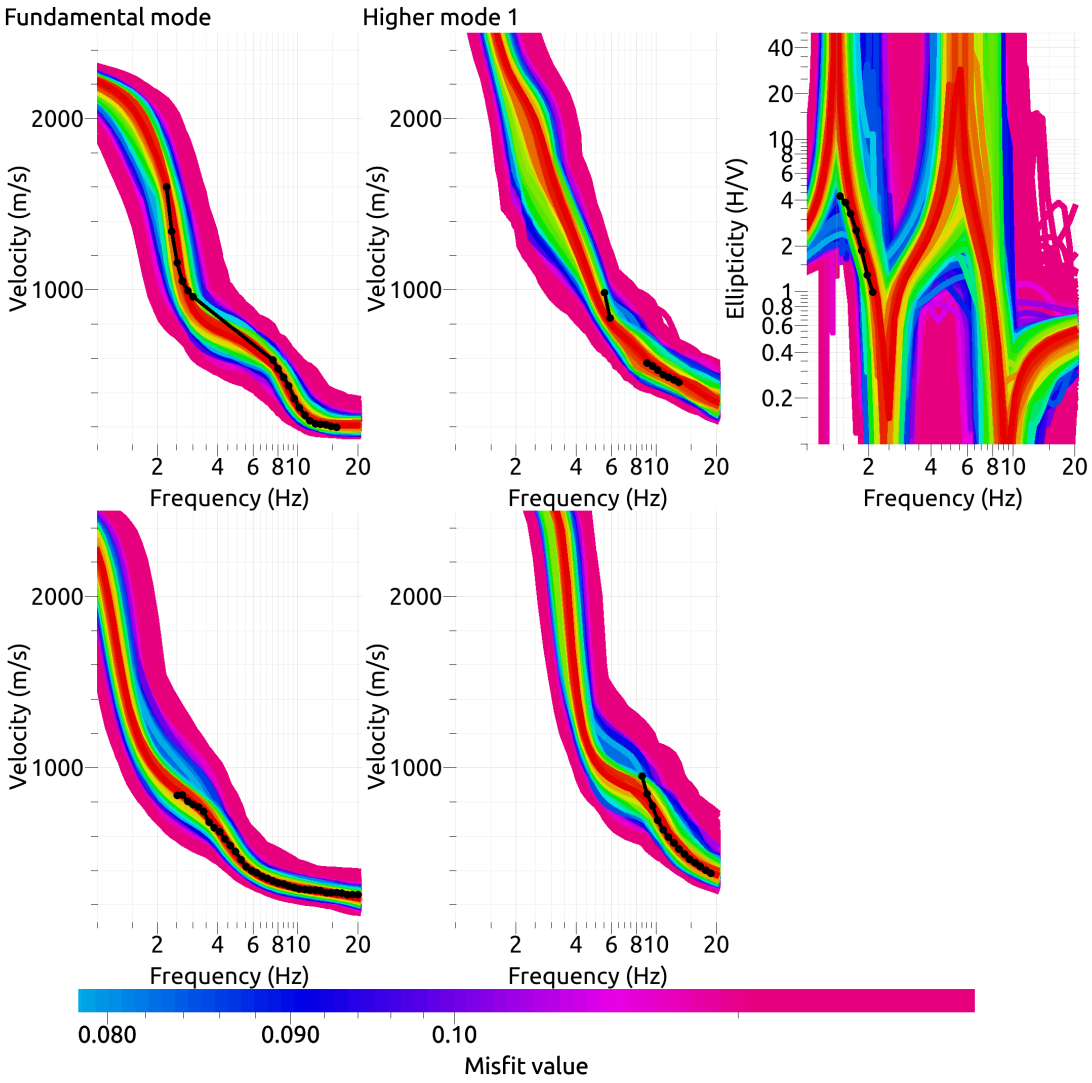

Figure 12: Comparison between inverted models and measured Rayleigh and Love modes and corresponding ellipticity, free layer depth strategy.

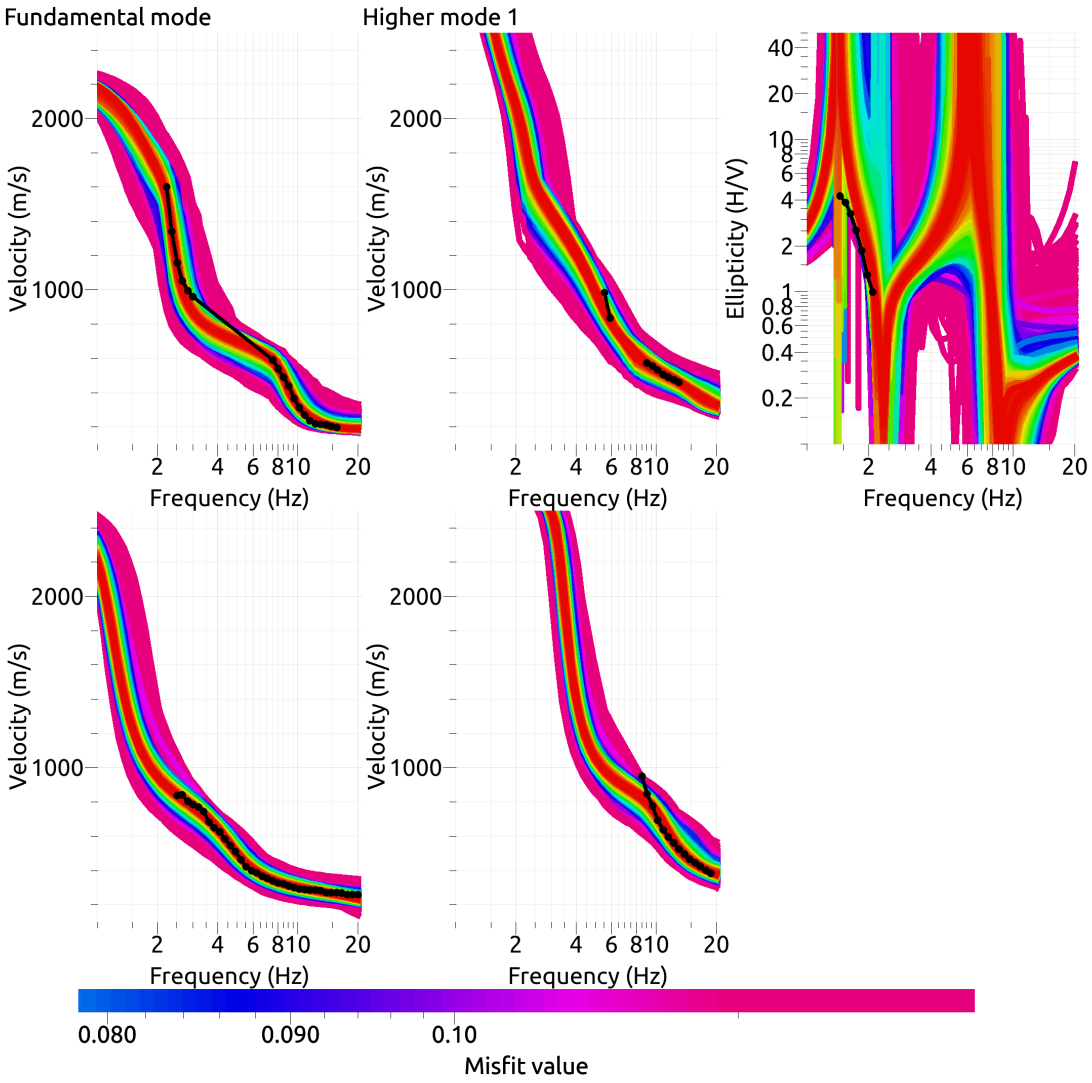

Figure 13: Comparison between inverted models and measured Rayleigh and Love modes and corresponding ellipticity, fixed layer depth strategy.

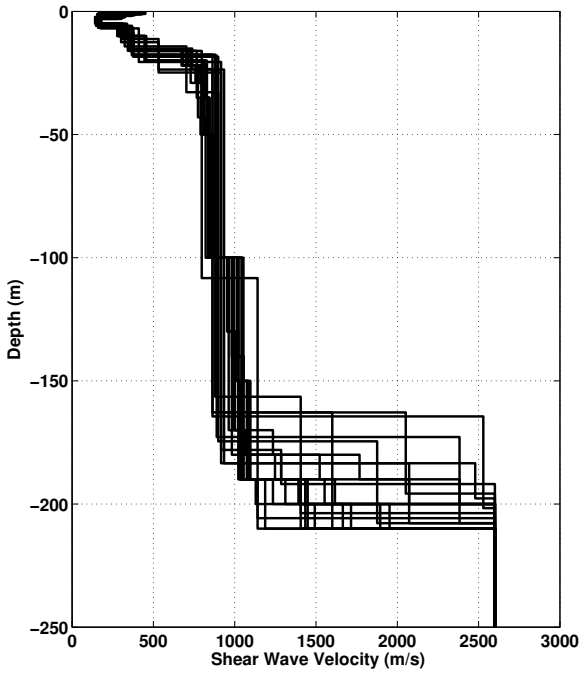

Figure 14: V_s ground profiles for the selected 25 best models.

[2012]. According to Rosselli [2001] who performed a gravimetric study on the Rhone valley, the sediments under station SBRS have a depth of about $100\,\mathrm{m}$, but they go down to $200\,\mathrm{m}$ slightly to the West.

Following Bard and Bouchon [1985] and Roten et al. [2006], the shape ratio for this valley is computed as $h/2w$, with h the maximal sediment thickness and $2w$ the valley width for which the sediment depth is larger than $h/2$. Considering the valley width of $1270\,\mathrm{m}$, $2w$ is most probably between the whole width and its half, most probably around $1000\,\mathrm{m}$. The maximum depth of the valley is estimated between 230 and $350\,\mathrm{m}$. It is therefore most probably between 0.2 and 0.5 here, with the highest probability around 0.3. The velocity contrast is defined as the bedrock velocity (between 1700 and $3000\,\mathrm{m/s}$, more likely $2600\,\mathrm{m/s}$) over the travel time average velocity into the sediments ($900\,\mathrm{m/s}$). It is therefore here between 1.9 and 3.3, most likely around 3.

This valley is therefore relatively shallow and wide and exhibits a velocity contrast that is not large enough, which places it more likely in the 1D behavior domain, according to Bard and Bouchon [1985] and Roten et al. [2006] (Fig. 15).

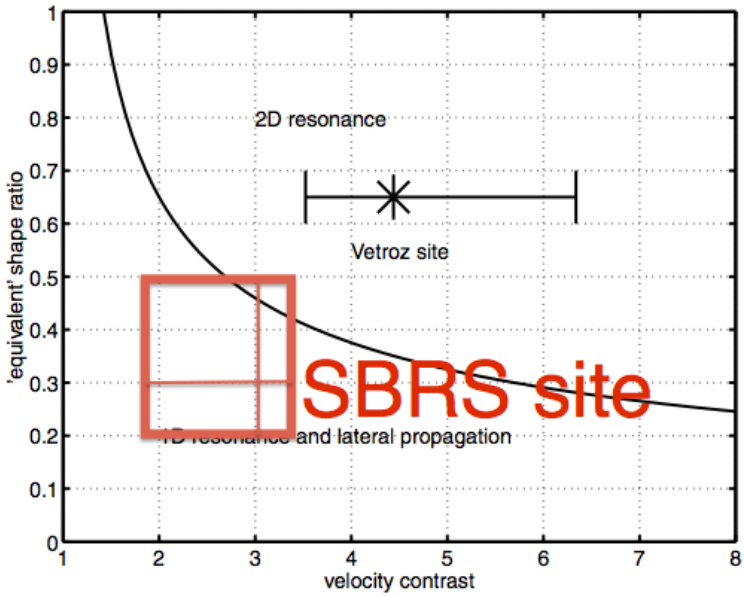

Figure 15: Theoretical behaviour of the Rhone valley at SBRS site compared to Vetroz site. Adapted from Roten et al. [2006]

6.2 Travel time average velocities and ground type

The distribution of the travel time average velocities at different depths was computed from the selected models. The uncertainty, computed as the standard deviation of the distribution of travel time average velocities for the considered models, is also provided, but its meaning is doubtful. $V_{s,30}$ is found to be $386\,\mathrm{m/s}$, meaning the site could be classified as class B in the Eurocode 8 [CEN, 2004], but considering the uncertainty and the measurement and the lithological description in EC8, it fits more with class C. For SIA261 [SIA, 2003], the first $20\,\mathrm{m}$ at about $400\,\mathrm{m/s}$ on top of better consolidated sediments with a velocity around $800\,\mathrm{m/s}$ would correspond to class E.

	Mean (m/s)	**Uncertainty (m/s)**
$V_{s,5}$	195	15
$V_{s,10}$	234	6
$V_{s,20}$	307	5
$V_{s,30}$	386	5
$V_{s,40}$	446	7
$V_{s,50}$	492	9
$V_{s,100}$	627	15
$V_{s,150}$	710	8
$V_{s,200}$	788	11

Table 7: Travel time averages at different depths from the inverted models. Uncertainty is given as one standard deviation from the selected profiles.

6.3 SH transfer function and quarter-wavelength velocity

The quarter-wavelength velocity approach [Joyner et al., 1981] provides, for a given frequency, the average velocity at a depth corresponding to 1/4 of the wavelength of interest. It is useful to identify the frequency limits of the experimental data (ellipticity peak at $1.4\,\mathrm{Hz}$ and minimum frequency in dispersion curves at $2.2\,\mathrm{Hz}$ here). The results using this proxy show that no data is controlling the results below $120\,\mathrm{m}$ and that the dispersion curves control the inversion down to $60\,\mathrm{m}$ (Fig. 16). Moreover, the quarter wavelength impedance-contrast introduced by Poggi et al. [2012a] is also displayed in the figure. It corresponds to the ratio between two quarter-wavelength average velocities, respectively from the top and the bottom part of the velocity profile, at a given frequency [Poggi et al., 2012a]. It shows a trough (inverse shows a peak) at the resonance frequency.
Moreover, the theoretical SH-wave transfer function for vertical propagation [Roesset, 1970] is computed from the inverted profiles. It is compared to the quarter-wavelength amplification [Joyner et al., 1981], that however cannot take resonances into account (Fig. 17). In this case, the models are predicting a large amplification at the secondary peaks, especially at 3.5 and $5\,\mathrm{Hz}$. This will be compared to observations at this station.

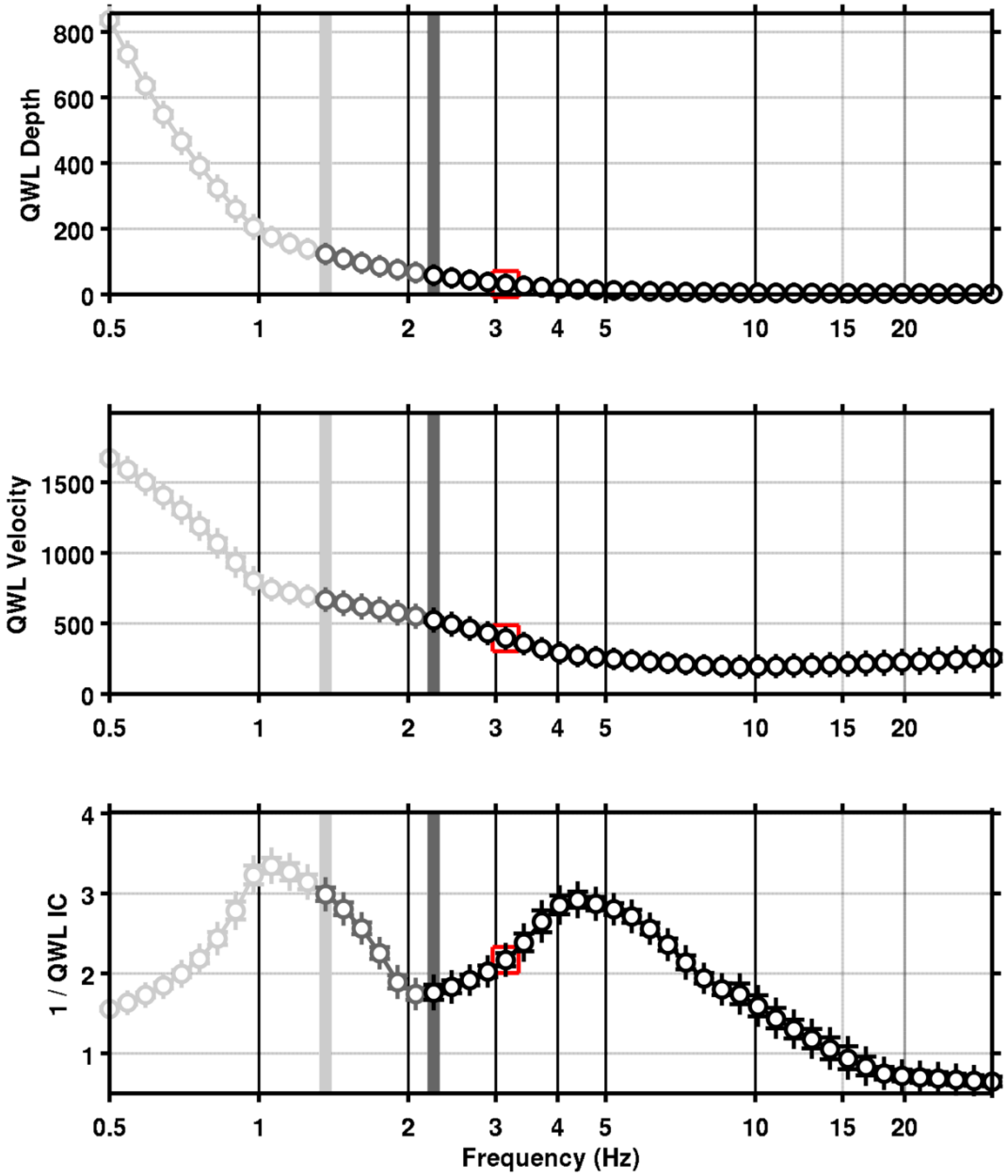

Figure 16: Quarter wavelength velocity representation of the velocity profile (top: depth, centre: velocity, bottom: inverse of the impedance contrast). Black curve is constrained by the dispersion curves, light grey is not constrained by the data. Red square is corresponding to $V_{s,30}$.

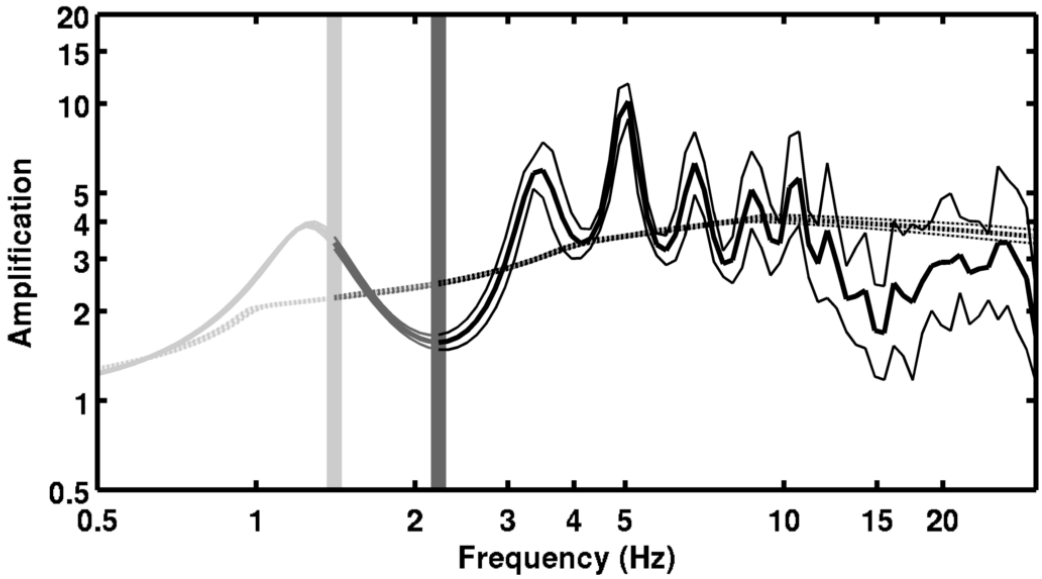

Figure 17: Theoretical SH transfer function (solid line) and quarter wavelength impedance contrast (dashed line) with their standard deviation. Significance of the greyshades is detailed in Fig. 16.

7 Conclusions

The array measurements presented in this study were successful in deriving a velocity model for the hospital site in Brig, below the SBRS station. We found the first 1 to $3\,\mathrm{m}$ with a larger velocity than the lower layers. Below the velocity remains extremely low until $5\,\mathrm{m}$ depth and then increases from 300 to $850\,\mathrm{m/s}$ at $20\,\mathrm{m}$ depth. In the lower layers, only a slight increase up to $1000\,\mathrm{m/s}$ is found until the bedrock between around $200\,\mathrm{m}$ with the imposed velocity of $2600\,\mathrm{m/s}$. $V_{s,30}$ is $386\,\mathrm{m/s}$. The ground type is C for EC8 and E for SIA261. The theoretical SH transfer function and impedance contrast of the quarter-wavelength velocity computed from the inverted profiles show a large amplification especially at the resonance frequencies 3.5 and $5\,\mathrm{Hz}$. Polarization in the valley axis was detected but it seems more likely that the behaviour of the valley is 1D. Recordings on the new station will allow to validate these simple models and recognize if 2D resonance occurs or not.

Acknowledgements

The authors thank Yaver Kamer for the help during these measurements.

References

Pierre-Yves Bard and Michel Bouchon. The Two-dimensional resonance of sediment-filled valleys. *Bulletin of the Seismological Society of America*, 75(2):519–541, 1985.

Sylvette Bonnefoy-Claudet, Fabrice Cotton, and Pierre-Yves Bard. The nature of noise wavefield and its applications for site effects studies. *Earth-Science Reviews*, 79(3-4): 205–227, December 2006. ISSN 00128252. doi: 10.1016/j.earscirev.2006.07.004. URL http://linkinghub.elsevier.com/retrieve/pii/S0012825206001012.

Jan Burjánek, Gabriela Gassner-Stamm, Valerio Poggi, Jeffrey R. Moore, and Donat Fäh. Ambient vibration analysis of an unstable mountain slope. *Geophysical Journal International*, 180(2):820–828, February 2010. ISSN 0956540X. doi: 10.1111/j.1365-246X.2009.04451.x. URL http://doi.wiley.com/10.1111/j.1365-246X.2009.04451.x.

J. Capon. High-Resolution Frequency-Wavenumber Spectrum Analysis. *Proceedings of the IEEE*, 57(8):1408–1418, 1969.

CEN. *Eurocode 8: Design of structures for earthquake resistance - Part 1: General rules, seismic actions and rules for buildings*. European Committee for Standardization, en 1998-1: edition, 2004.

Donat Fäh, Fortunat Kind, and Domenico Giardini. A theoretical investigation of average H / V ratios. *Geophysical Journal International*, 145:535–549, 2001.

Donat Fäh, Gabriela Stamm, and Hans-Balder Havenith. Analysis of three-component ambient vibration array measurements. *Geophysical Journal International*, 172(1):199–213, January 2008. ISSN 0956540X. doi: 10.1111/j.1365-246X.2007.03625.x. URL http://doi.wiley.com/10.1111/j.1365-246X.2007.03625.x.

Donat Fäh, Marc Wathelet, Miriam Kristekova, Hans-Balder Havenith, Brigitte Endrun, Gabriela Stamm, Valerio Poggi, Jan Burjanek, and Cécile Cornou. Using Ellipticity Information for Site Characterisation Using Ellipticity Information for Site Characterisation. Technical report, NERIES JRA4 Task B2, 2009.

Donat Fäh, Jeffrey R. Moore, Jan Burjánek, Ionut Iosifescu, Luis Dalguer, Fabrice Dupray, Clotaire Michel, Jochen Woessner, A. Villiger, Jan Laue, Iris Marschall, Valentin Gischig, Simon Loew, Alexandru Marin, Gabriela Gassner-Stamm, Sonia Alvarez-Rubio, Werner Balderer, Philipp Kästli, Domenico Giardini, C. Iosifescu, L. Hurni, Pierino Lestuzzi, Amin Karbassi, Cyrill Baumann, Alain Geiger, A. Ferrari, Lyesse Laloui, John Clinton, and Nicholas Deichmann. Coupled Seismogenic Geohazards in Alpine Region. *Bolletino di Geofisica Teorica ed Applicata*, 53(December):485–508, 2012. doi: 10.4430/bgta0048. URL http://www2.ogs.trieste.it/bgta/provapage.php?id_articolo=569.

William B. Joyner, Richard E. Warrick, and Thomas E. Fumal. The effect of Quaternary alluvium on strong ground motion in the Coyote Lake, California, earthquake of 1979. *Bulletin of the Seismological Society of America*, 71(4):1333–1349, 1981.

Katsuaki Konno and Tatsuo Ohmachi. Ground-Motion Characteristics Estimated from Spectral Ratio between Horizontal and Vertical Components of Microtremor. *Bulletin of the Seismological Society of America*, 88(1):228–241, 1998.

Valerio Poggi and Donat Fäh. Estimating Rayleigh wave particle motion from three-component array analysis of ambient vibrations. *Geophysical Journal International*, 180(1):251–267, January 2010. ISSN 0956540X. doi: 10.1111/j.1365-246X.2009.04402.x. URL http://doi.wiley.com/10.1111/j.1365-246X.2009.04402.x.

Valerio Poggi, Benjamin Edwards, and Donat Fäh. Characterizing the Vertical-to-Horizontal Ratio of Ground Motion at Soft Sediment-Sites. *Bulletin of the Seismological Society of America*, 102(6), 2012a. doi: 10.1785/0120120039.

Valerio Poggi, Donat Fäh, Jan Burjanek, and Domenico Giardini. The use of Rayleigh-wave ellipticity for site-specific hazard assessment and microzonation: application to the city of Lucerne, Switzerland. *Geophysical Journal International*, 188(3):1154–1172, March 2012b. ISSN 0956540X. doi: 10.1111/j.1365-246X.2011.05305.x. URL http://doi.wiley.com/10.1111/j.1365-246X.2011.05305.x.

J.M. Roesset. Fundamentals of soil amplification. In R. J. Hansen, editor, *Seismic Design for Nuclear Power Plants*, pages 183–244. M.I.T. Press, Cambridge, Mass., 1970. ISBN 978-0-262-08041-5. URL http://mitpress.mit.edu/catalog/item/default.asp?ttype=2\&tid=5998.

Alberto Rosselli. *Modélisation gravimétrique bi- et tridimensionnelle du substratum rocheux des vallées alpines - Applications à la Vallée du Rhône (Suisse), à la vallée de l'Adige (Italie) et au glacier de Lobbia (Italie).* PhD thesis, Université de Lausanne, 2001.

Daniel Roten, Donat Fäh, Cécile Cornou, and Domenico Giardini. Two-dimensional resonances in Alpine valleys identified from ambient vibration wavefields. *Geophysical Journal International*, 165(3):889–905, June 2006. ISSN 0956540X. doi: 10.1111/j.1365-246X.2006.02935.x. URL http://doi.wiley.com/10.1111/j.1365-246X.2006.02935.x.

SIA. *SIA 261 Actions sur les structures porteuses*. Société suisse des ingénieurs et des architectes, Zürich, sia 261:20 edition, 2003.

Marc Wathelet. An improved neighborhood algorithm: Parameter conditions and dynamic scaling. *Geophysical Research Letters*, 35(9):1–5, May 2008. ISSN 0094-8276. doi: 10.1029/2008GL033256. URL http://www.agu.org/pubs/crossref/2008/2008GL033256.shtml.